Sustainable Food Technology

ROYAL SOCIETY OF CHEMISTRY

PAPER

View Article Online
View Journal

Cite this: DOI: 10.1039/d6fb00083e

Decontamination of fresh wet rice noodles using a vertical in-package cold plasma system

Hongyu Long,[ab] Juhee Ahn,[ab] Tian Ding *[abc] and Xinyu Liao *[ab]

Fresh wet rice noodles (FWRNs) have high moisture and starch content, providing a suitable environment for microbial growth. In this study, an in-package dielectric barrier discharge (DBD) cold plasma system operating in a vertical mode was used for the decontamination of FWRNs. The effects of applied voltage, dielectric barrier thickness, discharge gap, electrode area, and package atmosphere on electrical behavior and microbial inactivation of this system were systematically investigated. Within a stable discharge regime, applied voltages above 70 kV, dielectric barrier thicknesses of 2–12 mm, discharge gaps of 30–45 mm, and electrode areas exceeding 50 cm^2 were found to be necessary to achieve sufficient charge transfer and effective microbial inactivation, suggesting a practical engineering window for scale-up design. Oxygen, air, and modified gases (65% O_2 + 10% N_2 + 25% CO_2 and 70% O_2 + 30% CO_2) enhanced the decontamination efficacy compared with pure nitrogen. During refrigerated storage at 4 °C, in-package DBD cold plasma-treated FWRNs maintained total plate counts below 5 log_{10} CFU g^{-1} for more than 16 days, significantly longer than conventional thermal pasteurization (~6 days), while better preserving textural properties, cooking quality, and visual appearance. Furthermore, a pilot-scale in-package DBD cold plasma system was constructed and validated for the decontamination of large-package FWRNs (300 g), indicating its potential to reduce microbial contamination and retard quality deterioration. Overall, these results provide essential insights linking reactor design, discharge characteristics, and microbial inactivation, supporting the development of scalable industrial in-package cold plasma equipment for commercial FWRN processing.

Received 18th March 2026
Accepted 15th June 2026

DOI: 10.1039/d6fb00083e

rsc.li/susfoodtech

Sustainability spotlight

In-package cold plasma processing offers a sustainable alternative to conventional thermal or chemical preservation methods. By effectively reducing microbial contamination while maintaining the quality of fresh wet rice noodles, the developed system extends the shelf life and helps reduce food loss, supporting sustainable and resource-efficient food processing.

1 Introduction

Fresh wet rice noodles (FWRNs) are widely consumed as a staple food in many regions, especially in Southeast Asia, owing to their convenience and nutritional value.[1] With high moisture content (typically 60–80%) and available nutrients,[2] FWRNs provide a suitable environment for microbial growth, particularly amylolytic bacteria (*e.g.*, *Bacillus* sp.), which can lead to spoilage and quality deterioration.[3] Thermal treatments have been applied for the decontamination of FWRNs.[4] However, high temperature might adversely affect their characteristics, such as clumping and strand breakage.[5] Moreover, post-thermal handling and packaging may introduce additional risks of microbial recontamination. Therefore, it is important to develop suitable nonthermal decontamination technologies to extend the shelf life and maintain the quality of FWRNs.

As a novel nonthermal decontamination technology, cold plasma has been increasingly applied in the field of food decontamination due to its high antimicrobial efficacy, no chemical residues and less damage to food quality.[6–8] In-package cold plasma is a specialized plasma approach in which plasma is generated directly inside a sealed package.[9] In this system, plasma reactive species are produced and retained within the package without the need for external gas supply, which is typically required in conventional cold plasma technologies.[10] When this package or the gas within is exposed to a strong electric field, a breakdown of the gas occurs, generating reactive species. Those species generated within the package then play important roles by interacting with the targeted

[a]College of Biosystems Engineering and Food Science, Zhejiang University, Hangzhou 310058, China. E-mail: tding@zju.edu.cn; xinyu_liao@zju.edu.cn
[b]Zhejiang Engineering Research Center of Flexible Intelligent Manufacturing for Food, Future Food Laboratory, Innovation Center of Yangtze River Delta, Zhejiang University, Jiaxing 314100, China
[c]Zhejiang Key Laboratory of Agri-food Resources and High-value Utilization, Zhejiang University, Hangzhou 310058, China

microorganisms, enclosed food products, and packaging materials. Due to their high diffusivity coefficients, these species rapidly diffuse into the pack ensuring uniform treatment.[11] Additionally, the in-package processing facilitates the storage of processed food products and offers a substantial potential for scaling up and commercialization.[9] The in-package cold plasma approach can reduce the risk of post-processing contamination introduced during post-treatment handling and packaging; moreover, it is compatible with modified-atmosphere packaging conditions and shows potential to achieve microbiological safety with limited impact on food quality.[9]

The in-package cold plasma systems have been widely reported for the microbial decontamination of various foods, including meat and meat products,[12,13] fruits and vegetables,[14,15] fish and fish products,[16,17] dairy products,[18,19] and rice-based products.[20,21] Most of the above studies remain at the laboratory scale, and the reactor configurations are predominantly based on horizontally arranged DBD dielectric plates. In particular, such designs may be unsuitable for continuous industrial-scale processing of soft-packaged products. Ziuzina *et al.*[10,22] developed an in-package cold plasma system called SAFEBAG for continuous processing of fresh cherry tomatoes, strawberries and spinach. Further systematic investigation of the relationships between reactor structural parameters—such as dielectric barrier thickness—and discharge characteristics, as well as their implications for microbial inactivation, is essential for establishing engineering guidelines to support equipment scale-up and industrial implementation.

The present study introduced a vertically configured in-package DBD cold plasma system and investigated the relationship between reactor geometry, electrical discharge characteristics, and microbial decontamination efficacy in FWRNs. By identifying suitable operating windows and parameter ranges, this work provided engineering data to support the development of continuous industrial-scale in-package cold plasma equipment. In addition, the preservation performance of this system was evaluated during refrigeration storage of FWRNs.

2 Materials and methods

2.1 Vertical in-package dielectric barrier discharge (DBD) plasma treatment system

The vertical in-package DBD plasma treatment system was developed based on Ziuzina *et al.*[10] with minor modifications. The packaged bags with FWRNs were vertically clamped between two ultra-high-molecular-weight polyethylene (UHMWPE) dielectric plates, each with an effective area of 36 cm × 50 cm. One plate was connected to the high-voltage electrode and the other to the ground electrode. Both electrodes were fabricated from 0.1 mm thick stainless-steel sheets. A high-voltage alternating current (AC) power supply (PSSBJ-5KVA/100 kV, Yangzhou Pinsheng Electric Co., Ltd, China) was applied to generate the plasma discharge. The system was operated and monitored *via* a microcomputer-based touchscreen power control console. As shown in Fig. 1, voltage waveforms across the DBD reactor and the monitor capacitor were recorded using a four-channel digital oscilloscope (DHO914S, Rigol, China). The discharge current was subsequently derived from the voltage across the monitor capacitor. For signal acquisition, the voltage waveform of the high-voltage electrode was recorded by feeding the signal from the U port, through a high-voltage probe, into channel CH1 of the oscilloscope. The voltage

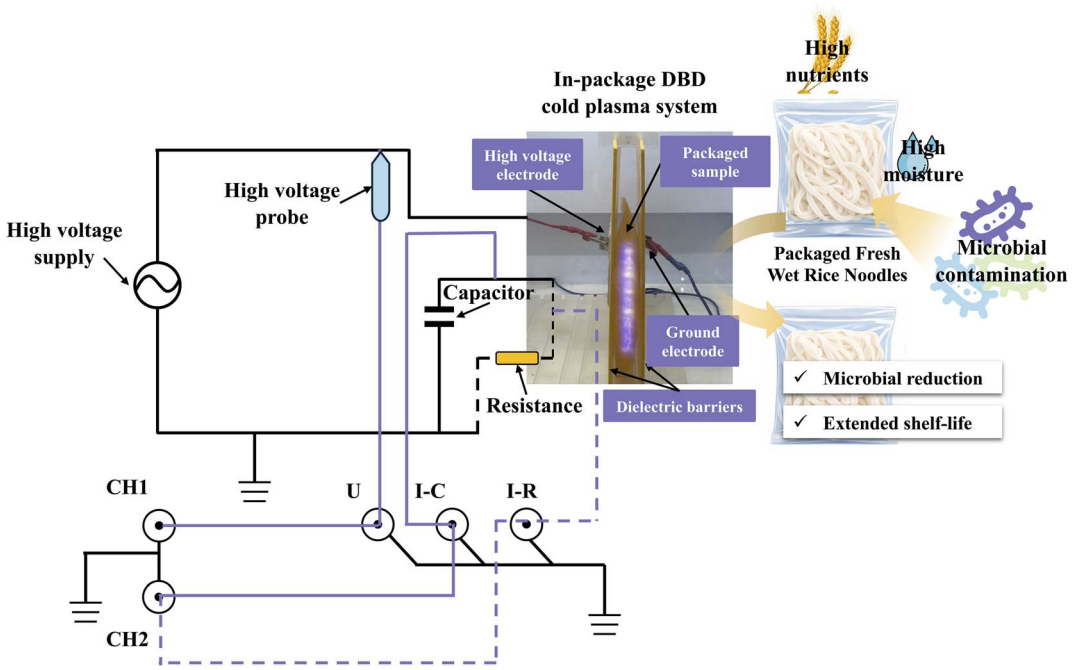

Fig. 1 Schematic of the in-package cold plasma system for the treatment of fresh wet rice noodles (FWRNs).

across the 0.01 μF monitor capacitor was fed from the *I–C* port to channel CH2 and was used to calculate the transferred charge *Q*; the discharge current was subsequently obtained from the temporal derivative of the charge. In an alternative configuration, a 1000 Ω sampling resistor was connected in series in the return path of the DBD reactor, and the voltage drop across this resistor was recorded using the oscilloscope as a voltage signal.

2.2 Electrical characteristic analysis

Under AC excitation, the discharge behavior of the DBD reactor was characterized using Lissajous plots and current–voltage waveforms. To obtain the Lissajous plots, a 0.01 μF sampling capacitor was connected in series in the return path of the DBD reactor. Because the equivalent capacitance of the DBD reactor was much smaller than that of the sampling capacitor, the voltage drop across the capacitor was negligible compared with the applied voltage, and the DBD reactor voltage could be approximated as the applied voltage measured using the high-voltage probe (Fig. 1). Accordingly, the reactor voltage *U*, obtained from the high-voltage probe with a division ratio of 10 000 : 1, was used as the *x*-axis of the Lissajous plots, while the transferred charge *Q* was calculated from the voltage across the monitor capacitor ($Q = C \times U_C$) by its capacitance and used as the *y*-axis. The area enclosed by each Lissajous loop corresponds to the energy dissipated in one AC cycle, and the average discharge power was calculated by multiplying this area by the driving frequency. The charge variation ΔQ over one cycle was used to quantify the effective discharge charge; in this study, the discharge charge (Q_d) was defined as the net charge transferred per cycle.[23]

In a complementary measurement, a 1000 Ω sampling resistor was connected in series in the return path of the DBD reactor. The voltage drop across this resistor was recorded using the oscilloscope and converted into the instantaneous discharge current using Ohm's law, allowing the construction of current–voltage (*I–V*) waveforms of the discharge. In a typical DBD process, the gap voltage increases within each half-cycle until the local electric field exceeds the breakdown threshold, leading to the formation of numerous short-lived filamentary microdischarges in the gas gap, which appear as sharp current spikes in the waveform. The current pulse number is the number of distinguishable transient current spikes observed in the discharge current waveform within one applied AC voltage cycle. By analyzing the number, peak amplitude, and temporal distribution of these current pulses in each cycle, the intensity, uniformity, and stability of the discharge can be assessed.[23] The Lissajous plots provide information on the discharge power and discharge charge from energy and charge-transfer perspectives, while the *I–V* waveforms reveal the evolution of microdischarge behavior, thus offering a comprehensive characterization of the DBD plasma discharge process.

2.3 Preparation of *Bacillus cereus*

Glycerol stocks of *Bacillus cereus* ATCC 14579 were streaked onto Mannitol–Egg Yolk–Polymyxin (MYP) agar plates (Qingdao Hope Bio-Technology, Qingdao, China) and incubated at 37 °C for 24 h. A single colony was then inoculated into fresh Luria–Bertani (LB) broth (Qingdao Hope Bio-Technology, Qingdao, China) and incubated at 37 °C overnight with shaking at 150 rpm. The cells were subsequently harvested by centrifugation at 6000 rpm for 10 min at 4 °C and resuspended in sterile 0.85% physiological saline to reach a cell concentration of around 9 $\log_{10}$ CFU mL^{-1} for further experiments.

2.4 Microbial inoculation and packaged FWRN preparation

FWRNs (200 g) were rinsed with sterile distilled water and then immersed in a *B. cereus* suspension for 20 min to allow microbial inoculation. The noodles were subsequently removed and dried under airflow in a laminar-flow cabinet for 20 min until no visible surface moisture remained. The inoculated noodles were then aseptically portioned (10 g per bag) and packed into sterile packaging bags (20 cm × 30 cm, 0.16 mm thickness). The packaging material consisted of a polypropylene/polyethylene terephthalate (PP/PET) multilayer film. The bags were filled with air, oxygen (O_2), nitrogen (N_2), or gas mixtures (65% O_2 + 10% N_2 + 25% CO_2 and 70% O_2 + 30% CO_2), followed by gas flushing and heat sealing using a packaging machine (1002D, Hefei Huahao Technology Co., Ltd, China).

2.5 In-package DBD and pasteurization treatments of packaged FWRNs

To assess the effect of an in-package DBD system on microbial inactivation in FWRNs, a series of processing parameters were systematically investigated, including treatment time, applied voltage, dielectric plate thickness, discharge gap, electrode area, gas composition, and gas filling volume. *B. cereus* was selected as the target bacterium.

The treatment times were set at 30, 60, 90, 120, and 150 s, with applied voltages of 60, 70, and 80 kV. Dielectric plates with thicknesses of 4, 6, 8, 10, 12, and 14 mm were used, and discharge gaps were adjusted to 30, 35, 40, 45, and 50 mm. Electrode areas of 15, 25, 50, 100, 200, and 300 cm^2 were evaluated. The packages were filled with air, pure oxygen (O_2), nitrogen (N_2), or gas mixtures (65% O_2 + 10% N_2 + 25% CO_2 and 70% O_2 + 30% CO_2), with gas filling volumes of 1130 mL.

For conventional thermal pasteurization, packaged FWRNs were immersed in a water bath at 65 °C for 30 min, 75 °C for 5 min, or 85 °C for 15 s, followed by immediate removal for further analysis.

To evaluate the effects of different treatments on shelf life, both treated and untreated FWRN samples were stored at 4 °C under refrigerated conditions. Subsamples were collected at predetermined time intervals for microbiological enumeration of the total bacterial counts and mold and yeast counts, as well as for quality analyses.

2.6 Microbiological analysis of FWRN samples

For the determination of *B. cereus* inactivation, both treated and untreated FWRN samples (10 g) were aseptically transferred into 90 mL of sterile 0.85% physiological saline and thoroughly homogenized. Tenfold serial dilutions were then prepared and spread-plated on MYP agar. The plates were incubated at 37 °C

for 24 h, and *B. cereus* colonies were enumerated and expressed as colony-forming units (CFU) to evaluate the inactivation efficiency of the in-package DBD treatment.

For shelf-life evaluation during refrigerated storage, microbiological analyses of FWRNs were performed in accordance with Chinese national standard methods for total plate count (TPC; GB 4789.2-2022)[24] and for mold and yeast counts (GB 4789.15-2016).[25] Briefly, 25 g of packaged FWRNs were aseptically transferred into 225 mL of sterile 0.85% physiological saline and homogenized to obtain an initial 10^{-1} suspension. Tenfold serial dilutions were subsequently prepared, and 1 mL aliquots of appropriate dilutions were inoculated into sterile Petri dishes. Plate Count Agar (PCA) was used for TPC determination, while Rose Bengal Agar (RBA) was used for mold and yeast enumeration. PCA plates were incubated at 37 °C for 48 h, and RBA plates were incubated at 28 °C for 5 days. Microbial counts were recorded and expressed as CFU per gram (CFU g^{-1}) of FWRN sample.

2.7 Quality analysis of packaged FWRNs

2.7.1 Determination of water content and water activity (a_w) of FWRNs. The water content of FWRNs was determined using a rapid moisture analyzer (HKSF-2, Wuxi Huake Instrument and Meter Co., Ltd, China).[26] Approximately 5 g of FWRNs was evenly distributed on the sample pan and measured according to the manufacturer's instructions until a stable reading was obtained. Water activity (a_w) was measured using a water activity meter (AquaLab 4, Decagon Devices, Inc., USA) at 25 °C.[27] Approximately 5 g of FWRNs was placed in the sample cup and measured until the a_w value stabilized. All measurements were performed in triplicate for each treatment and sampling time. Moisture content and water activity were determined to assess changes in the water status of FWRNs during storage under different treatments.

2.7.2 Textural analysis of FWRNs. Texture profile analysis (TPA) was performed according to Chen *et al.* (2019),[26] with minor modifications. The textural characteristics of FWRNs were measured using a texture analyzer (TMS-PRO, Food Technology Corporation, USA) operated in texture profile analysis mode. For each measurement, three noodle strands with a suitable length (approximately 15 cm, slightly longer than the test platform) were aligned in parallel on the test platform. A cylindrical probe with a diameter of 75 mm was used at a test speed of 1 mm s^{-1}, with a deformation of 50% and a trigger force of 5 g. Each sample was subjected to two consecutive compression cycles with a brief interval between compressions. Measurements were performed in at least three replicates for each treatment at each storage time. From the resulting force–time curves, hardness, adhesiveness, springiness, cohesiveness and chewiness were calculated to characterize the textural changes of FWRN during storage under different treatments.

2.7.3 Determination of cooking quality of FWRNs. Approximately 2 g of FWRNs were accurately weighed (m_0) and cooked in boiling distilled water at a noodle-to-water ratio of 1 : 50 (g : mL) for 60 s with gentle stirring. Cooking loss was determined by evaporating the cooking water to constant weight and expressed as the percentage of dry matter lost relative to the initial sample weight (dry basis).[28]

Under the same cooking conditions, cooked noodle strands were randomly selected from each sample, gently lifted from the middle, and held horizontally for around 10 s. The numbers of broken strands and total strands were recorded, and the cooked breakage rate (CBR) was expressed as the percentage of broken noodle strands relative to the total number of noodle strands.[28] Each sample was measured in at least three replicates, and the mean values of CL and BR were used to evaluate the effects of in-package DBD and thermal treatments on the cooking performance and structural stability of FWRNs.

2.7.4 Visual assessment of FWRNs. The visual appearance of FWRNs subjected to different treatments was monitored during the storage period. For each treatment and sampling day, representative samples were photographed in a small photographic light box under standardized background and lighting conditions. All images were captured from a fixed vertical distance of 56.5 cm to ensure consistency.

2.8 Pilot-scale feasibility study of continuous in-package DBD cold plasma processing of FWRNs

To evaluate the feasibility of scaling up the in-package DBD cold plasma treatment for industrial applications, a pilot-scale continuous processing system was constructed based on the laboratory-scale reactor described in Section 2.1 and integrated with a conveyor belt transport system. The conveyor belt enabled continuous movement of packaged FWRN samples through the plasma discharge zone between the dielectric plates, allowing simulation of industrial continuous processing conditions. The conveyor belt speed was adjusted to control the effective plasma exposure time of the packaged samples. Two conveyor speeds were evaluated: 0.066 m s^{-1}, corresponding to an effective treatment time of approximately 15 s, and 0.033 m s^{-1}, corresponding to an effective treatment time of approximately 30 s. The applied voltages were set at 80 kV and 90 kV, respectively. Compared with the laboratory-scale experiments, the electrode area was expanded to 2000 cm^2 in order to provide a larger discharge region suitable for pilot-scale processing. For the pilot-scale trials, each packaging bag contained 300 g of FWRNs, which is comparable to the typical commercial packaging specification of fresh wet rice noodles. During operation, the packaged FWRN samples were placed on the conveyor belt and transported through the plasma discharge region between the dielectric plates, where in-package plasma was generated under atmospheric pressure. After treatment, the samples were stored at 4 °C and collected every 5 days for subsequent microbiological and quality analyses to preliminarily assess the scalability and practical applicability of the continuous in-package DBD cold plasma process for FWRN preservation.

2.9 Statistical analysis

Statistical analyses were conducted using GraphPad Prism 9.0 (GraphPad Software, San Diego, CA, USA). Differences among groups were analyzed by one-way analysis of variance (ANOVA),

followed by Tukey's multiple comparison test. Statistical significance was defined at $p < 0.05$.

3 Results and discussion

3.1 Reactor parameters and discharge atmospheres on electrical characteristics and microbial inactivation in an in-package DBD cold plasma system

3.1.1 Applied voltage. Adjusting the input voltage is one of the most common ways to regulate the performance of in-package DBD cold plasma processing. As shown in Fig. 2, increasing the applied voltage led to a rise in the discharge charge (Q_d, Fig. 2A) and discharge power (Fig. 2B), accompanied by an enlargement of the parallelogram area of the Q–V Lissajous loops (Fig. 2C). At higher applied voltages, the current waveforms exhibited more frequent pulses with higher amplitudes (Fig. 2D). This phenomenon can be attributed to the enhanced electric field strength in the discharge gap, which promotes electron acceleration and impact ionization, thereby generating more intense filamentary microdischarges and increasing charge transfer within each applied AC voltage cycle (Fig. 2E). Regarding the microbial decontamination performance, the inactivation levels of *B. cereus* in FWRNs were enhanced with increasing applied voltage (Fig. 2F). After a 150 s in-package DBD cold plasma treatment, the reduction level of *B. cereus* reached 2.87 $\log_{10}$ CFU g^{-1} at an applied voltage of 60 kV and exceeded 4 $\log_{10}$ CFU g^{-1} when the applied voltage was enhanced to 70 or 80 kV. The increased discharge charge and the higher frequency of current pulses indicate intensified filamentary discharge activity, which is expected to promote the production of plasma reactive species and increase their interaction with microbial cells inside the package.[12] Applied voltage of above 70 kV is required for this in-package cold plasma system.

3.1.2 Dielectric layer thickness. The thickness of the dielectric layers is one important structural parameter governing the discharge behavior of in-package DBD cold plasma systems. As shown in Fig. 3A–E, increasing the dielectric layer (UHMWPE plate) thickness led to a decrease in the transferred charge, discharge power, and current pulse activity, reflecting a concomitant weakening of the effective electric field strength in the discharge gap. This decrease can be mainly attributed to the reduced capacitive coupling and increased electrical impedance of the DBD reactor when a thicker dielectric barrier was used. At a fixed applied voltage, a thicker dielectric layer limited charge transfer within each applied AC voltage cycle, thereby reducing the Q–V Lissajous loop area and the discharge power. In addition, the reduced charge transfer weakened the development of filamentary microdischarges in the gas gap, resulting in fewer and lower-amplitude current pulses. Therefore, increasing the dielectric barrier thickness diminishes both the intensity and frequency of filamentary microdischarges.[29–31] This electrical behavior is reflected in the microbial inactivation performance, whereby thicker dielectric plates led to weaker discharge intensity and, consequently, reduced efficacy. As shown in Fig. 3A–C, when the barrier thickness reached approximately 12 mm, further increases resulted in insignificant enhancements in the attenuation of discharge intensity, and the Lissajous figure deviated from the canonical capacitive parallelogram (Fig. 3D), indicating a transition toward a less ideal discharge regime.[32]

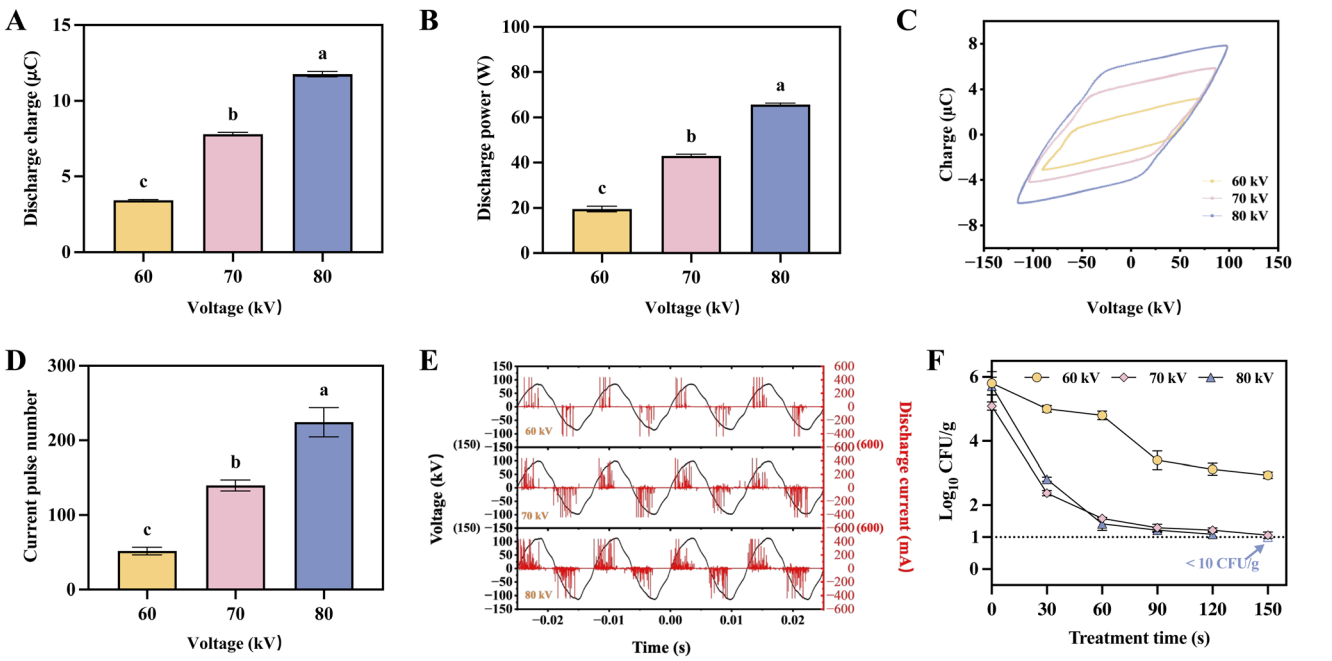

Fig. 2 Effects of applied voltage on the electrical characteristics and antimicrobial performance of the in-package DBD cold plasma system: (A) discharge charge, (B) discharge power, (C) Q–V Lissajous loops, (D) current pulse number, (E) I–V characteristics, and (F) inactivation of *Bacillus cereus* in fresh wet rice noodles (FWRNs).

Conversely, an excessively thin barrier can also compromise discharge stability and structural integrity of the reactor. As shown in Fig. 3F, when the dielectric plate thickness was reduced to 2 mm, pronounced inward deformation was observed in the region adjacent to the electrode after a 60 s discharge. During plasma operation, part of the input energy was consumed in gas ionization, while the remaining portion was dissipated as thermal energy.[33,34] For a thin dielectric layer, localized electrode heating combined with electrostatic stress led to substantial mechanical deformation. Accordingly, a practical design window of approximately 3–12 mm for the dielectric barrier thickness can be established under the present reactor configuration and operating conditions.

Within this range, the antimicrobial performance of in-package DBD cold plasma on FWRNs under various dielectric barrier thicknesses is exhibited in Fig. 3G. When the barrier layer thickness was 4 mm, the population of *B. cereus* counts decreased by 3.96 $\log_{10}$ CFU g^{-1}, while the reduction decreased to 3.52 $\log_{10}$ CFU g^{-1} when the thickness increased to 8 mm after a 60 s in-package DBD cold plasma processing, indicating a decline in microbial inactivation efficiency with increasing thickness.

Therefore, the suitable dielectric thickness was selected based on the consideration of discharge intensity, microbial inactivation, insulation reliability, and operational stability. Although a thinner dielectric barrier favored stronger discharge and higher microbial inactivation efficiency, an excessively thin barrier could cause structural deformation and unstable discharge during high-voltage operation. In contrast, an excessively thick barrier reduced the charge transfer, discharge power, and current pulse activity, thereby weakening microbial inactivation. Based on this balance, dielectric layers in the range of 4–6 mm were considered as a preferred operating region for

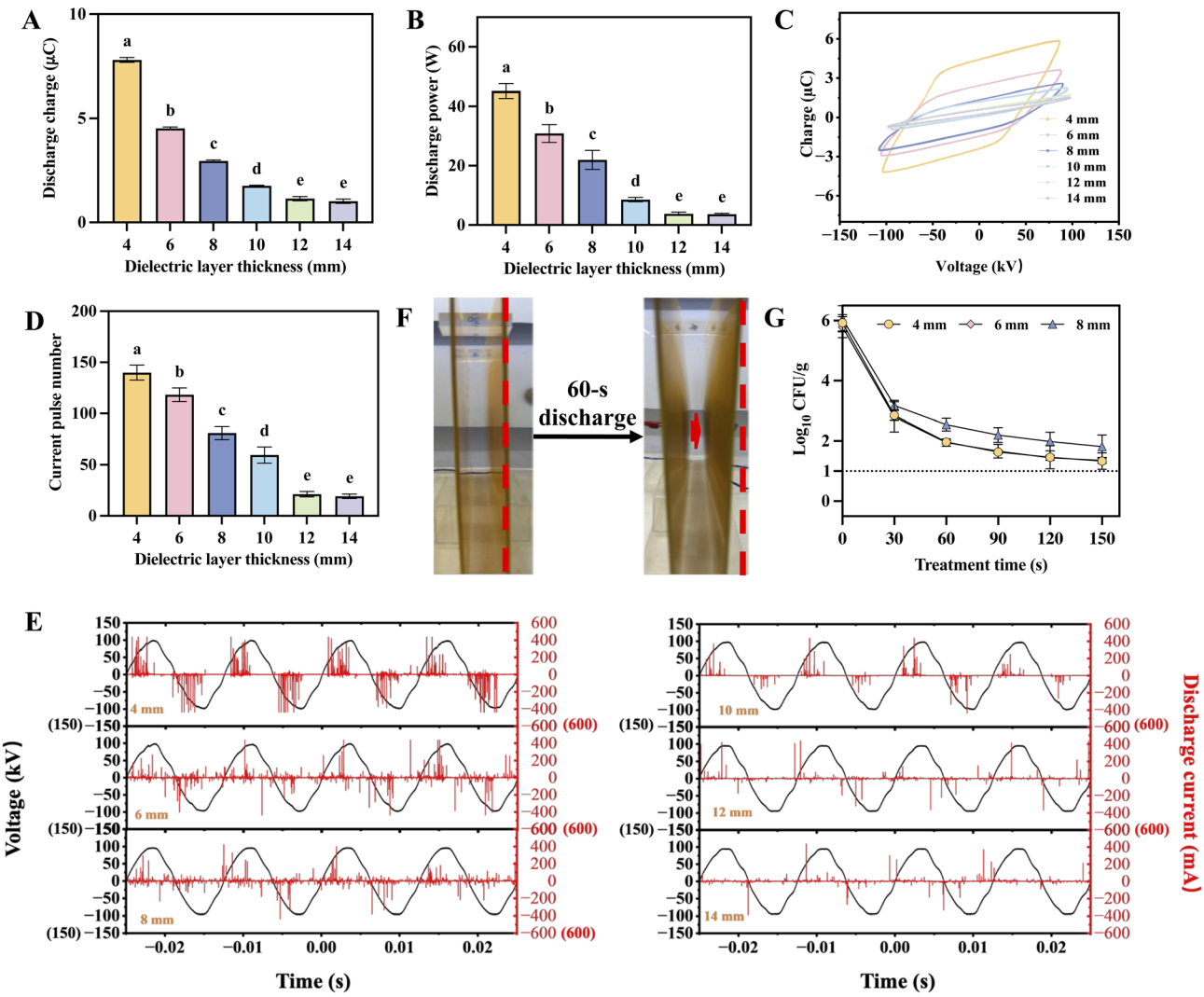

Fig. 3 Effects of dielectric layer thickness on the electrical characteristics and antimicrobial performance of the in-package DBD cold plasma system: (A) discharge charge, (B) discharge power, (C) *Q*–*V* Lissajous loops, (D) current pulse number, (E) *I*–*V* characteristics, (F) structural deformation of the dielectric barrier (2 mm thickness) after a 60 s plasma discharge, and (G) inactivation of *Bacillus cereus* in fresh wet rice noodles (FWRNs).

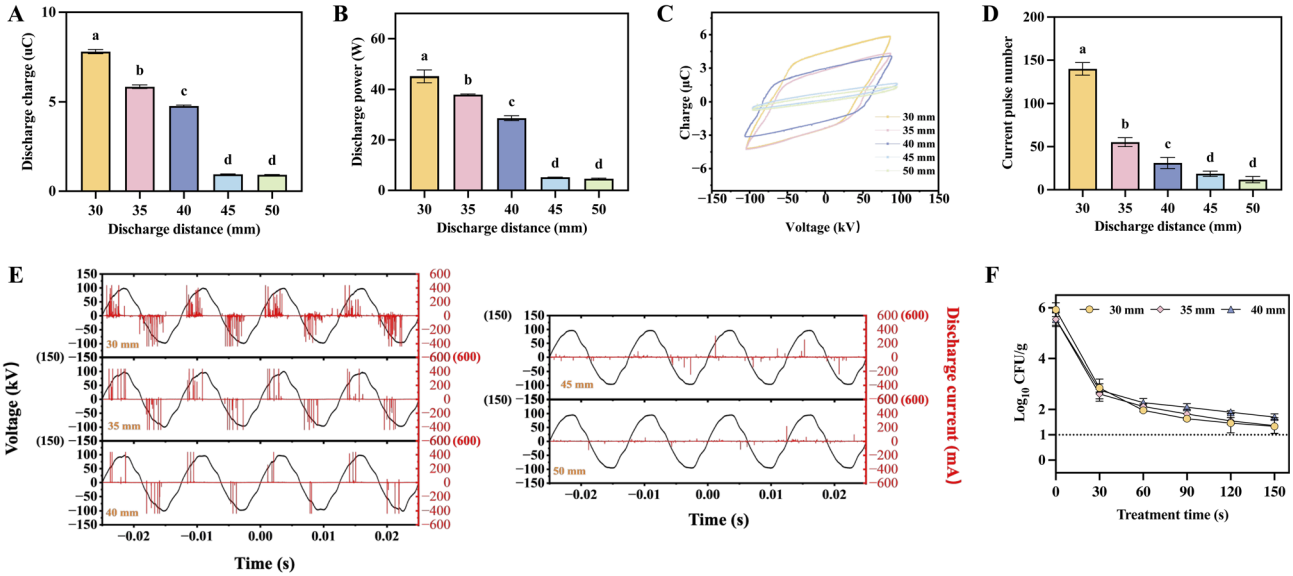

Fig. 4 Effects of discharge distance on the electrical characteristics and antimicrobial performance of the in-package DBD cold plasma system: (A) discharge charge, (B) discharge power, (C) *Q–V* Lissajous loops, (D) current pulse number, (E) *I–V* characteristics, and (F) inactivation of *Bacillus cereus* in fresh wet rice noodles (FWRNs).

the configuration development of the in-package DBD cold plasma system.

3.1.3 Discharge distance. The discharge distance between the dielectric plates is another geometrical parameter governing the discharge behavior of the DBD reactor.

When the reactor was approximated as an equivalent capacitor and the applied voltage amplitude was kept constant (at the power-supply setting), increasing the gas gap altered the electric field distribution. This led to a decrease in the effective capacitance of the system and consequently reduced the charge transferred per cycle.[32] In this study, increasing the discharge gap from 30 to 35 and 40 mm led to significant reductions in discharge charge, discharge power, and current pulse activity (Fig. 4A–E). This decrease in current pulse activity is associated with reduced effective electric field strength and limited charge transfer at larger discharge distances. As the gas gap increased, gas breakdown became more difficult to achieve within each applied voltage cycle, thereby suppressing the formation and development of filamentary microdischarges. Consequently, fewer and lower-amplitude current pulses were observed in the discharge waveform. When the discharge distance was further increased to 45 and 50 mm, the number of current pulses dropped sharply (Fig. 4E), and the enclosed area of the *Q–V* Lissajous loops shrank dramatically, deviating from the characteristic parallelogram shape (Fig. 4C), indicating weakened discharge activity and reduced energy deposition. Based on these results, it can be inferred that, under the present operating conditions, the discharge distance should be kept below approximately 45 mm to maintain stable plasma generation. However, for in-package food treatment, the discharge distance cannot be arbitrarily reduced, as sufficient space must be reserved between the dielectric plates to accommodate the gas-filled package. For the packaged FWRNs used in this study, a minimum discharge distance of 30 mm was required to ensure adequate spatial clearance. Regarding the microbial efficacy, as shown in Fig. 4F, the in-package DBD cold plasma system with a discharge distance of 30 mm achieved a reduction of around 4.30 $\log_{10}$ CFU g^{-1} of *Bacillus cereus* after a 90 s treatment, whereas larger discharge distances of 35 and 40 mm resulted in lower reductions of 3.73 and 3.46 $\log_{10}$ CFU g^{-1}, respectively.

Therefore, the discharge distance should be optimized by balancing package accommodation, plasma stability, discharge intensity, and microbial inactivation efficiency. A shorter discharge distance within the practical clearance range favors stronger electric-field-driven discharge, higher discharge power, and more active filamentary microdischarges, which promote the generation of RONS and enhance their interactions with microbial cells inside the package. In contrast, an excessively large discharge distance reduces plasma generation and energy deposition, thereby limiting RONS generation and reducing microbial inactivation efficiency.

3.1.4 Electrode area. In in-package DBD cold plasma systems, electrode area is an important structural parameter affecting the reactor capacitance, discharge power, and current pulse behavior. Increasing the electrode area can enhance the equivalent capacitance of the reactor, as described by the capacitance relationship ($C \propto S/d$).[35] At a fixed applied voltage, a larger electrode area allows the system to store and transfer a greater amount of charge per cycle, thereby enlarging the *Q–V* Lissajous loop area and increasing the discharge power. In addition, a larger effective electrode area provides broader active discharge region and increases the probability of filamentary microdischarges, leading to a higher current pulse number. However, for a given power supply, the electrode area cannot be increased indefinitely. When the electrode area is too

large and approaches the edge of the dielectric plate, the creepage distance may become insufficient, increasing the risk of edge discharge, unstable discharge, or even arcing. These phenomena can interfere with the normal discharge process and reduce the operational stability of the reactor.

As shown in Fig. 5A–C, decreasing the electrode area led to reductions in transferred charge, discharge power, and the progressive compression of the *Q*–*V* Lissajous loops. The current pulse number decreased accordingly, as exhibited in Fig. 5D and E. When the electrode area was reduced to approximately 25 cm^2, the discharge characteristics exhibited no significant differences compared with those observed at 15 cm^2. Therefore, an electrode area of at least approximately 25 cm^2 was identified as a practical lower bound for the in-package DBD cold plasma system design in this study.

As shown in Fig. 5F, when the electrode area was increased from 100 cm^2 to 300 cm^2, the reduction of *B. cereus* was enhanced from 3.81 log_{10} CFU g^{-1} to 4.30 log_{10} CFU g^{-1} after 90 s of treatment. The enhanced microbial inactivation at larger electrode areas can be attributed to the enlarged effective discharge region, improved spatial coverage, and increased generation of reactive species, which enhanced the probability of interactions between plasma-generated reactive species and microorganisms within the package. These results suggest that electrode area is a key parameter when developing the scale-up in-package DBD cold plasma processing. However, during scale-up, the electrode area should be increased together with appropriate power supply capacity while maintaining sufficient creepage distance and dielectric safety margin to ensure stable plasma generation and effective microbial inactivation.

3.1.5 Gas composition. In addition to electrical discharge parameters, the composition of the gas enclosed within the package plays a critical role in determining the antimicrobial efficacy of in-package DBD cold plasma systems. As exhibited in Fig. 6, nitrogen as the working gas resulted in only approximately a 1 log reduction during the first 30 s of treatment, after which no further significant inactivation was observed. Oxygen, air, 65% O_2 + 10% N_2 + 25% CO_2, and 70% O_2 + 30% CO_2 resulted in a higher reduction of *B. cereus* in FWRNs. This may be attributed to differences in plasma chemistry associated with the working gas composition. Previous studies have shown that DBD plasmas operated in oxygen-rich or CO_2 containing atmospheres generate higher concentrations of strongly oxidizing reactive species such as ozone, hydroxyl radicals and singlet oxygen,[36,37] which play key roles in microbial inactivation. Considering both the antimicrobial efficacy and practical implementation cost, air was therefore selected as the working gas for subsequent shelf-life evaluation experiments.

3.2 Batch in-package DBD cold plasma for the preservation of FWRNs during refrigeration storage

3.2.1 Microbiological changes in FWRNs during storage. Fig. 7 shows the effects of the in-package DBD cold plasma system on the TPC, as well as mold and yeast counts in FWRNs during 16 days of refrigerated storage. On day 0, the TPC of untreated FWRNs was approximately 3.31 log_{10} CFU g^{-1}. Following pasteurization treatments (65 °C/30 min, 75 °C/5 min, and 85 °C/15 s) and in-package cold plasma treatment (80 kV/150 s), the TPC values decreased to 1.98, 2.18, 2.72 and 2.09 log_{10} CFU g^{-1}, respectively (Fig. 7A). During refrigerated storage, the TPC of untreated FWRNs increased rapidly, exceeding 5 log_{10} CFU g^{-1} by 8 days, which may be attributed to the high moisture content and water activity of the product.[3] The TPC of those treated by pasteurization at 65 °C/30 min and 85 °C/15 s increased over 5 log_{10} CFU g^{-1} at 14 and 10 days, respectively. In contrast, FWRNs subjected to pasteurization at

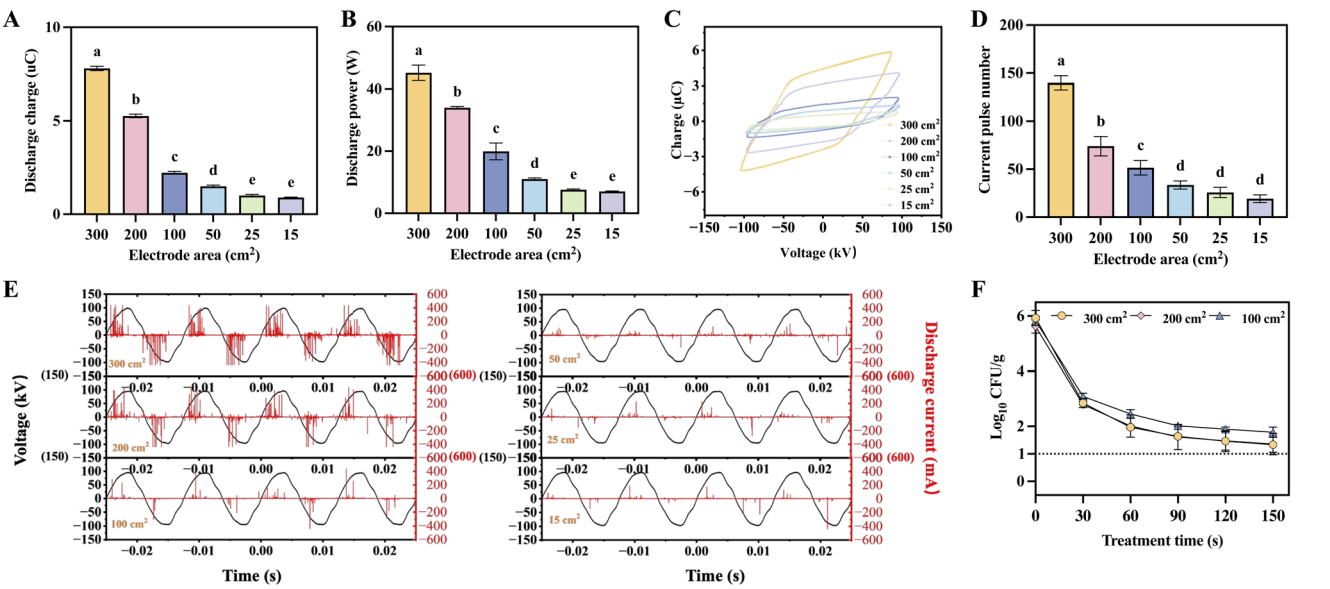

Fig. 5 Effects of electrode area on the electrical characteristics and antimicrobial performance of the in-package DBD cold plasma system: (A) discharge charge, (B) discharge power, (C) *Q*–*V* Lissajous loops, (D) current pulse number, (E) *I*–*V* characteristics, and (F) inactivation of *Bacillus cereus* in fresh wet rice noodles (FWRNs).

75 °C/5 min or in-package cold plasma treatment (80 kV/150 s) maintained TPC values below 5 $\log_{10}$ CFU g^{-1} throughout the 16-day storage period. Regarding the mold and yeast counts, the initial population in FWRNs was approximately 1.18 $\log_{10}$ CFU g^{-1} on day 0 and increased to around 2.55 $\log_{10}$ CFU g^{-1} by day 16 in the untreated samples. In contrast, pasteurization and in-package cold plasma treatments reduced mold and yeast counts to below the limit of detection during storage (Fig. 7B). The antimicrobial effect of in-package cold plasma is associated with the generation of RONS, which play key roles in microbial inactivation.[32,38]

3.2.2 Water content and a_w changes in FWRNs during storage. The quality and stability of FWRNs are closely associated with their water content and the interaction between water molecules and other constituents, which could influence the structural characteristics of the product.[39] As shown in Fig. 8A, on day 0, no significant differences in water content were observed between the treated samples and the untreated FWRNs (62.65%) ($p > 0.05$). During refrigerated storage at 4 °C, the moisture content of FWRNs in all groups gradually decreased. This decrease may be attributed to a combination of factors, including microbial growth and metabolic activity, as well as moisture redistribution and evaporation during storage.[40] Compared with thermal pasteurization treatments, the in-package DBD cold plasma treatment maintained water content and water activity at comparable levels during storage, indicating that plasma treatment did not induce additional moisture loss.

Water activity (a_w) reflects the thermodynamic availability of water for microbial growth and is closely related to shelf-life stability.[41] As exhibited in Fig. 8B, the a_w of FWRNs in all groups decreased slowly from values close to 1.00 to approximately 0.984–0.990 during refrigerated storage, remaining in a high-a_w range without significant differences ($p > 0.05$) among different treatments. Previous studies have reported that FWRNs, as high-moisture, high-a_w starch gels, undergo water migration from the interior matrix toward the surface and headspace during storage.[42] This process is often accompanied by starch retrogradation and syneresis, leading to progressive decreases in both moisture content and a_w,[42] which is consistent with the overall trends observed in this study.

3.2.3 pH changes in FWRNs during storage. As shown in Fig. 9, on day 0, the pH value of untreated FWRNs was 6.51, and thermal pasteurization resulted in only slight variations in the pH value, ranging from 6.36 to 6.58. However, the pH value of FWRNs treated with in-package DBD cold plasma treatment decreased to 4.62, which may be associated with the generation of RONS during plasma discharge. These reactive species can interact with the surface of FWRNs and contribute to the formation of acidic compounds such as nitric acid and nitrous acid, leading to a decrease in pH.[43] During the refrigeration storage, the pH value of all the FWRN samples showed a decreasing trend (Fig. 9). This reduction might be attributed to microbial metabolism, in which microorganisms utilize available carbohydrates and produce organic acids, leading to acidification of FWRNs as the storage time was extended.[44]

3.2.4 Texture profile changes in FWRNs during storage. The changes in the texture profile of FWRNs are exhibited in Fig. 10. On day 0, the hardness value of untreated FWRNs was 40.81 N, and it decreased to 16.59, 18.23 and 34.26 N after 65 °C/30 min, 75 °C/5 min and 80 °C/15 s thermal pasteurization treatments, respectively (Fig. 10A). Thermal pasteurization can cause the absorption of free water present on the surface of FWRNs, leading to secondary starch gelatinization and a consequent reduction in noodle hardness.[45] However, in-package cold plasma treated FWRNs exhibited a slightly higher hardness value of 41.90 N compared with the untreated samples. This behavior may be associated with plasma-induced modifications of the noodle matrix. Abundant RONS within the package may induce oxidative cross-linking between starch and protein chains, contributing to denser and more compact microstructure of noodles.[46] In addition, plasma treatment may induce slight moisture redistribution or localized dehydration, which can reduce moisture-mediated plasticization and thereby contribute to the maintenance of noodle firmness. During refrigerated storage at 4 °C, as shown in Fig. 10A, the hardness of untreated, pasteurized treated and plasma-treated FWRNs increased rapidly in the early period of 8 days, which might be attributed to the starch retrogradation.[47] As the storage time was extended further, the hardness of FWRNs tended to decrease. It reduced from 62.13 N on day 8 to 49.11 N on day 16 for the untreated FWRNs (Fig. 10A), which might be attributed to the growth of microorganisms, producing enzymes to hydrolyze proteins and starch.[5] Cohesiveness represents the internal structural integrity of the noodle matrix.[48] As exhibited in Fig. 10B, there were no significant changes in the values of cohesiveness of FWRNs with various treatments, and the values remained relatively stable throughout storage.

Springiness indicates the ability to recover its shape after deformation.[48] On day 0, the springiness of untreated and thermally treated FWRNs ranged from 1.14 to 1.24 mm without significant differences (Fig. 10C). However, it significantly increased to 1.56 mm after in-package cold plasma treatment ($p < 0.05$), which might be attributed to plasma-induced

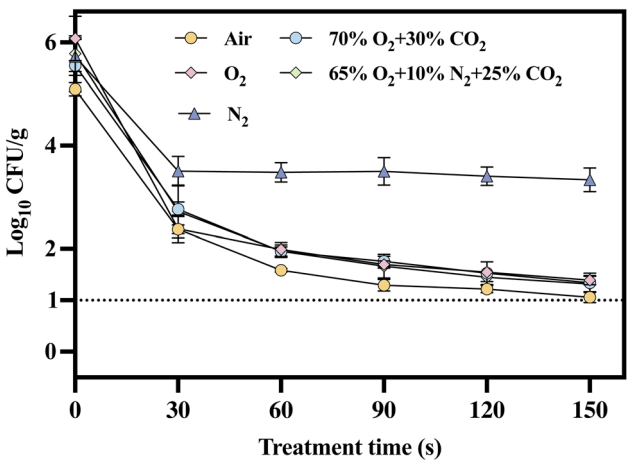

Fig. 6 Effects of gas compositions on the antimicrobial performance of the in-package cold plasma system on *Bacillus cereus* in fresh wet rice noodles (FWRNs).

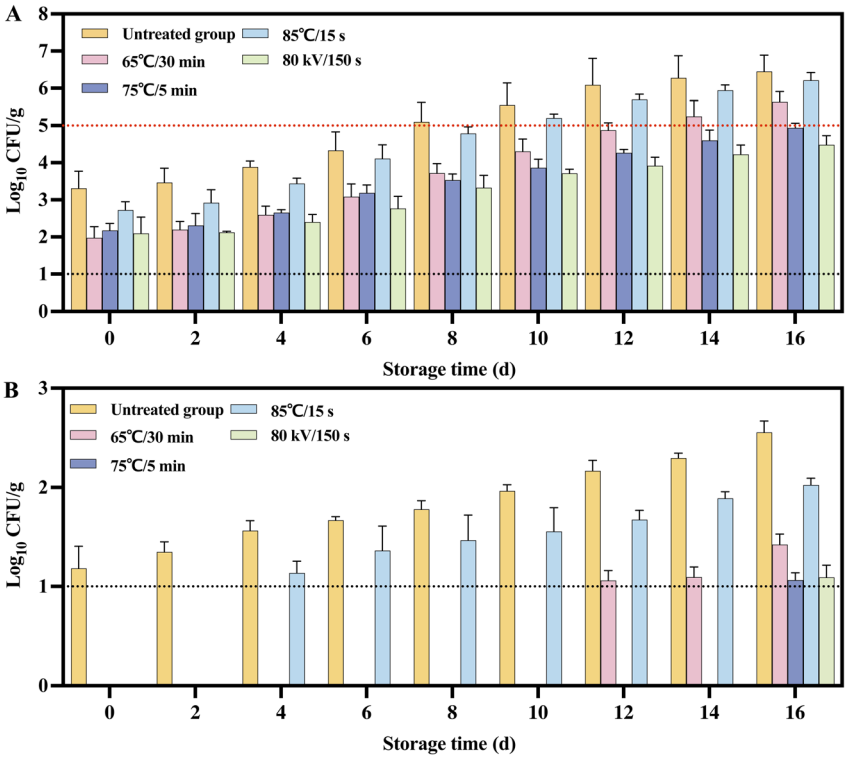

Fig. 7 Changes in (A) total plate count (TPC) and (B) mold and yeast counts of packaged fresh wet rice noodles (FWRNs) with different treatments during storage at 4 °C.

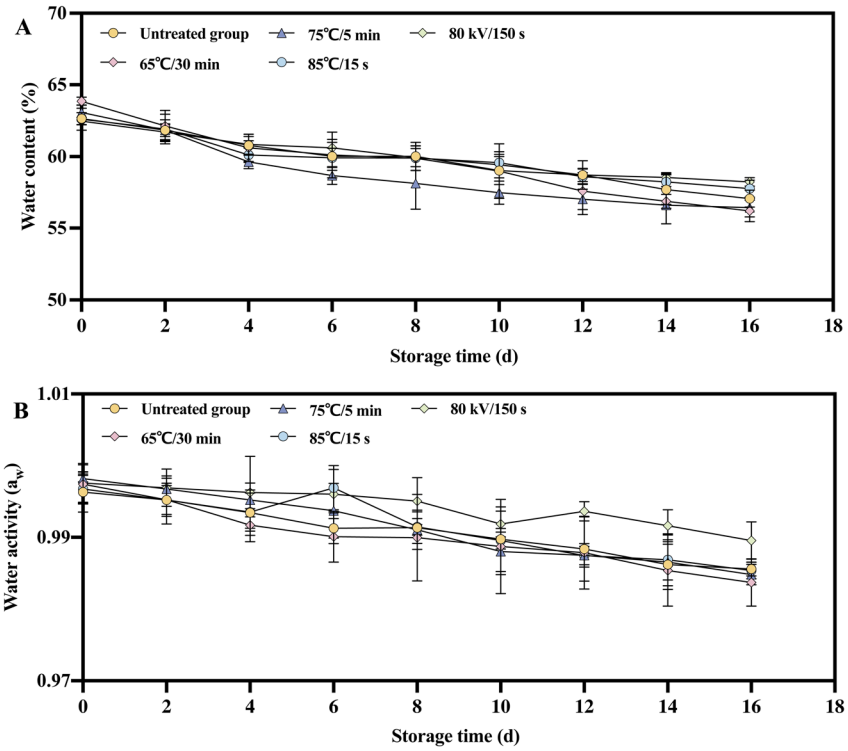

Fig. 8 Changes in (A) water content (%) and (B) water activity (a_w) of packaged fresh wet rice noodles (FWRNs) with various treatments during storage at 4 °C.

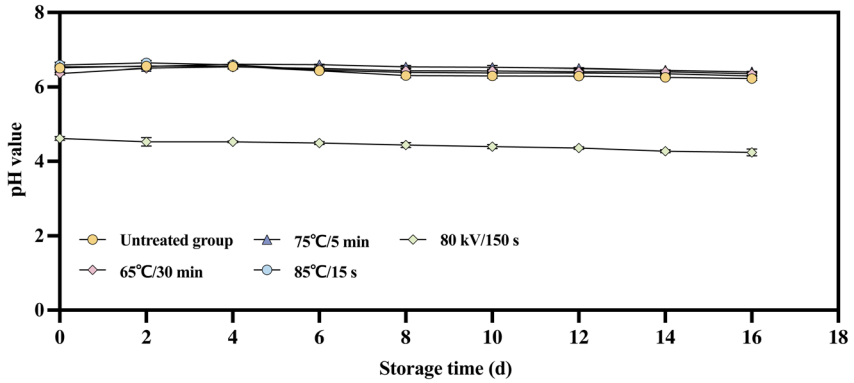

Fig. 9 Changes in pH value of packaged fresh wet rice noodles (FWRNs) with various treatments during storage at 4 °C.

modifications of the noodle matrix. During the refrigeration storage, the springiness of FWRNs with different treatments increased initially and then retained relative stable.

Gumminess is defined as the product of hardness and cohesiveness.[46] On day 0, the gumminess value of untreated and plasma-treated FWRNs was 28.49 N and 32.17 N, respectively. In contrast, thermal pasteurization treatments resulted in decreases in the gumminess of FWRNs, especially at 65 °C/30 min, 75 °C/5 min (Fig. 10D). This decrease in gumminess following thermal processing can be attributed to heat-induced water uptake and further starch gelatinization, which soften the gel matrix and reduce resistance to breakdown during compression. In contrast, in-package cold plasma is a nonthermal process that does not induce thermal softening; instead, plasma-induced modifications and limited moisture redistribution may help maintain the integrity of the starch gel network, resulting in comparable or slightly higher gumminess values. During storage, the gumminess property of FWRNs with various treatments generally increased, following a trend similar to that of hardness.

Chewiness is a composite parameter reflecting the energy required to masticate the noodles.[49] Before storage, the untreated FWRNs retained a chewiness value of 35.24 mJ, and in-package cold plasma processing did not result in a significant change in chewiness (Fig. 10E). However, the values decreased to 14.53 mJ, 15.25 mJ, and 28.59 mJ after 65 °C/30 min, 75 °C/5 min and 80 °C/15 s thermal pasteurization treatments, respectively. During the refrigeration storage, as exhibited in Fig. 10E, the chewiness of FWRNs with various treatments increased, largely following the trend observed for hardness and gumminess, implying that structural strengthening contributed to increased chewing resistance.

3.2.5 Cooking property changes in FWRNs during storage. The cooking loss rate is an important indicator of the quality of FWRNs, reflecting the levels of material loss during cooking.[40,50] A high cooking loss is undesirable. As shown in Fig. 11A, during refrigerated storage at 4 °C, the cooking loss of FWRNs with various treatments increased over time. The cooking loss of untreated FWRNs increased from 0.33% to 2.53%, which might be associated with disintegration of the rice flour gel structure, moisture migration and solid leaching.[51,52] Samples subjected to thermal treatments maintained lower cooking loss, ranging from 0.75 to 1.46% throughout the storage period. The reduction in cooking loss induced by heating may be attributed to the changes in the multiscale and pore structures of the rice noodles, which enhanced water penetration into the interior and reduced structural damage during cooking.[53] Regarding the in-package DBD cold plasma treatment, the cooking loss remained below 1% at the end of the refrigerated storage at 4 °C, which may be attributed to plasma-induced surface and interfacial modifications that enhance the structural integrity of the noodle matrix and limit the leaching of soluble components during cooking. In addition, the nonthermal nature of plasma processing avoids excessive gelatinization or thermal softening,[54] thereby helping to maintain structural stability and reduce cooking-induced breakdown.

On day 0, the cooked breakage rate of untreated FWRNs was 1.96%, and it increased to 9.53%, 7.82%, and 3.44% after 65 °C/30 min, 75 °C/5 min and 85 °C/15 s thermal treatments, respectively (Fig. 11B). The cooked breakage rate of FWRNs treated with in-package DBD cold plasma increased slightly to 2.46%. In addition, the cooked breakage rates of FWRNs in all groups increased with extended storage time. Based on QB/T 2652-2025 (Rice Noodles), the cooked breakage rate of FWRNs should be below 10%.[55] As shown in Fig. 11B, the values of untreated or thermally treated FWRNs exceeded 10% by day 8, while plasma-treated FWRNs remained at 6.07%. Unlike cooking loss, which mainly reflects solute leaching during cooking, cooked breakage rate is more closely related to the macroscopic integrity and brittleness of the starch gel network. Moderate thermal treatments may reduce cooking loss by forming a denser structure while promoting starch chain rearrangement and increased molecular ordering,[56] which may contribute to increased brittleness and a tendency to break after cooking.

3.2.6 Appearance changes in FWRNs during storage. Daily photographs of FWRNs with various treatments were taken to assess the appearance changes during refrigerated storage at 4 °C. As shown in Fig. 12A, the untreated FWRNs exhibited strand adhesion, dull color, and the appearance of visible mold spots after 10 days of storage. Surface stickiness, loss of brightness, and mold growth are closely associated with rapid microbial proliferation under high-moisture, high-aw conditions of FWRNs.[57] For thermally treated samples (65 °C/30 min and 75 °C/5 min), swelling and partial deformation of noodle strands

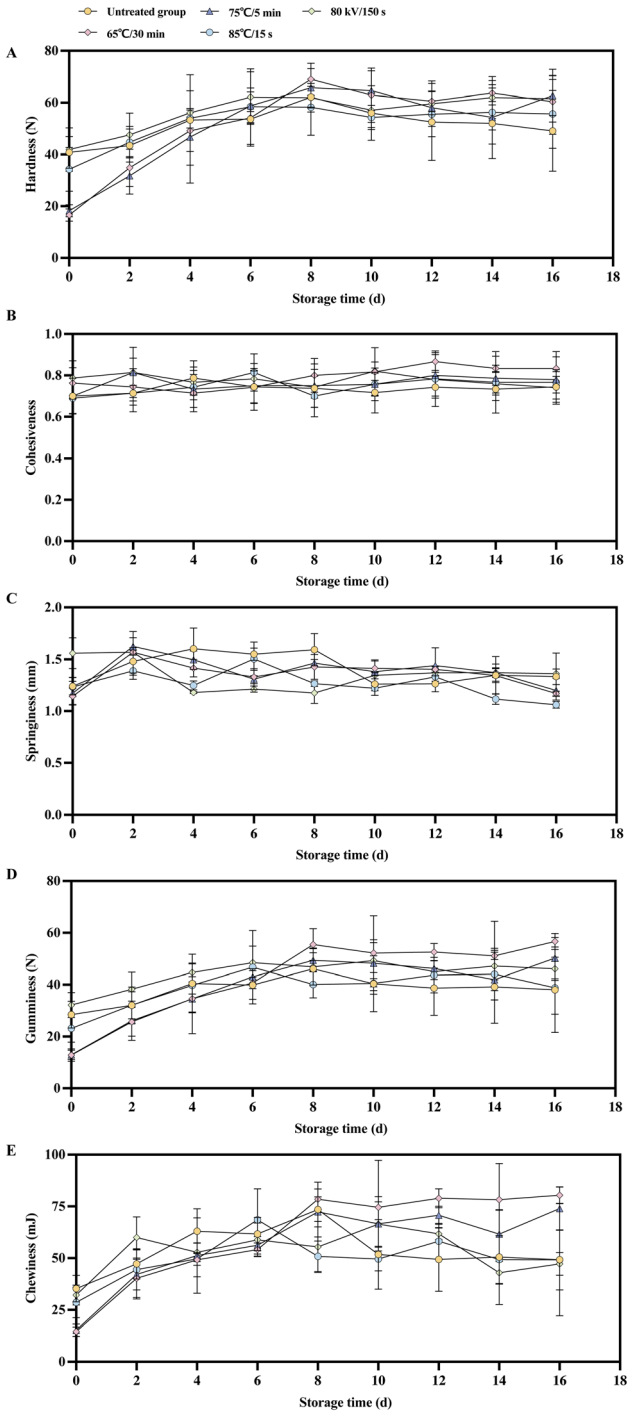

Fig. 10 Changes in the texture characteristics of packaged fresh wet rice noodles (FWRNs) with various treatments during storage at 4 °C: (A) hardness, (B) cohesiveness, (C) springiness, (D) gumminess, and (E) chewiness.

were observed during storage, indicating deterioration in appearance. This behavior is consistent with the texture profile analysis results, where thermal treatments induced softening effects, including reduced hardness and gumminess, likely due to moisture redistribution and further starch gelatinization. In contrast, FWRNs treated with in-package DBD cold plasma retained a more intact strand structure and relatively stable color throughout the storage period, exhibiting only minor surface drying at the final time points (Fig. 12E). This visual stability was in agreement with the texture analysis results, which showed that the hardness, cohesiveness, springiness, and gumminess remained relatively stable in plasma-treated samples. The nonthermal nature of plasma processing likely contributes to improved structural integrity and reduced surface stickiness, thereby preserving both the appearance and textural properties of FWRNs during refrigerated storage (Fig. 12E).

3.3 Pilot-scale feasibility study of continuous in-package DBD cold plasma processing of FWRNs

Based on the laboratory-scale results, an applied voltage above 70 kV, a dielectric barrier thickness of 2–12 mm, a discharge gap of 30–45 mm, and electrode areas exceeding 50 cm^2 were required to achieve sufficient charge transfer and effective microbial inactivation, indicating a practical engineering window for pilot-scale design. A pilot-scale study was further conducted to preliminarily evaluate the applicability of the continuous in-package DBD cold plasma process for the decontamination of large package FWRNs at various conveyor belt speeds. To characterize the pilot-scale system, its electrical properties, including discharge power and current pulse behavior, were also evaluated, as shown in Fig. 13. To meet the requirements of pilot-scale processing, the electrode area was enlarged to around 2000 cm^2. A dielectric thickness of 10 mm and a discharge gap of 40 mm were selected to maintain discharge stability while accommodating the larger packaged products. In this way, the smaller-scale batch study did not merely provide isolated operating conditions but also offered a basis for pilot-scale development. Specifically, the batch study demonstrated how the applied voltage, dielectric thickness, discharge distance, and electrode area influenced the discharge intensity, current pulse activity, reactor stability, and antimicrobial efficacy. These results suggested a practical parameter window in which effective plasma generation could be achieved without unstable discharge, excessive attenuation, or structural limitations. During pilot-scale development, this parameter window was not directly copied but adapted according to the engineering requirements of a continuous large-package system. In particular, the enlarged electrode area was adopted to extend treatment coverage, while the dielectric thickness and discharge gap were selected to maintain stable filamentary microdischarge behavior and sufficient spatial clearance under the larger reactor geometry. Meanwhile, the conveyor speed served as an additional scaling-up factor that regulated the residence time. Accordingly, the role of the laboratory-scale study was to identify the governing parameters and acceptable operating boundaries of the in-package DBD reactor, whereas the role of the pilot-scale study was to verify the robustness and applicability of this parameter window under larger packages, an expanded treatment area, and continuous conveyor operation.

As exhibited in Fig. 14A, the TPC of untreated FWRNs was 1.90 $\log_{10}$ CFU g^{-1}, and after pilot-scale plasma treatment on

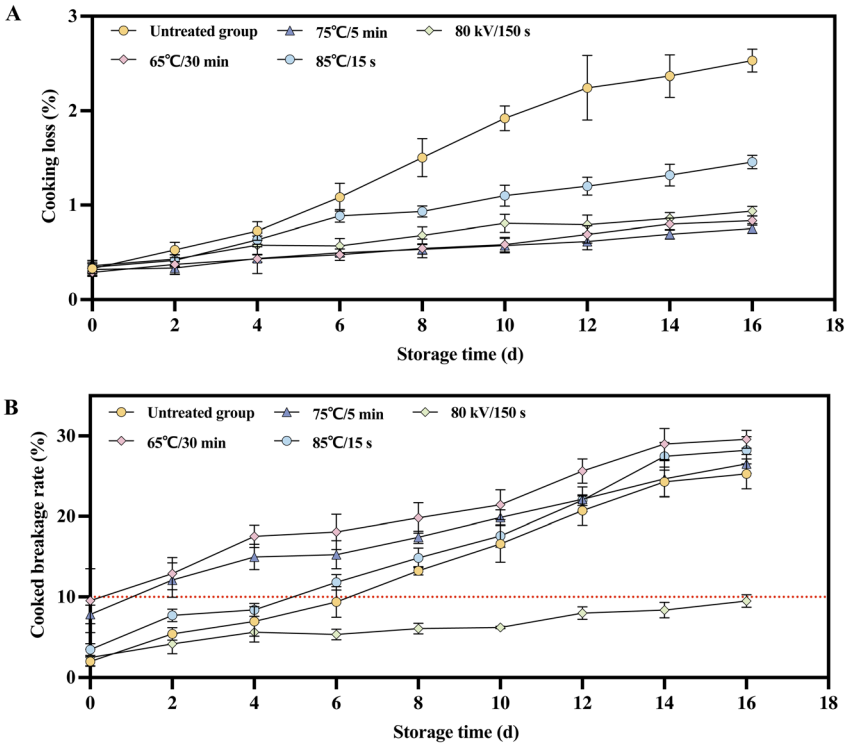

Fig. 11 Changes in (A) cooking loss (%) and (B) cooked breakage rate (%) of packaged fresh wet rice noodles (FWRNs) with various treatments during storage at 4 °C.

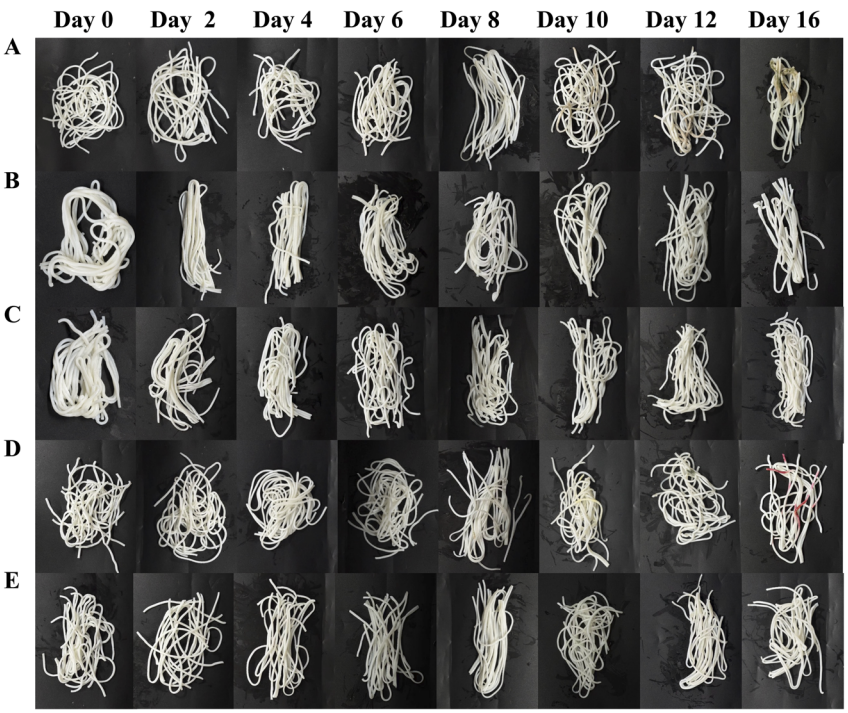

Fig. 12 Changes in the appearance of packaged fresh wet rice noodles (FWRNs) with various treatments during storage at 4 °C: (A) untreated noodles, (B) 65 °C/30 min-treated noodles, (C) 75 °C/5 min-treated noodles, (D) 85 °C/15 s-treated noodles, and (E) 85 kV/150 s-treated noodles.

day 0, the TPC decreased to a range of 1.52–1.79 $\log_{10}$ CFU g^{-1}. During storage, the untreated group exhibited a continuous increase in TPC, reaching 5.08 $\log_{10}$ CFU g^{-1} after 10 days. In contrast, all plasma-treated FWRN samples retained values lower than 5 $\log_{10}$ CFU g^{-1}, indicating that in-package DBD plasma treatment effectively delayed microbial growth during

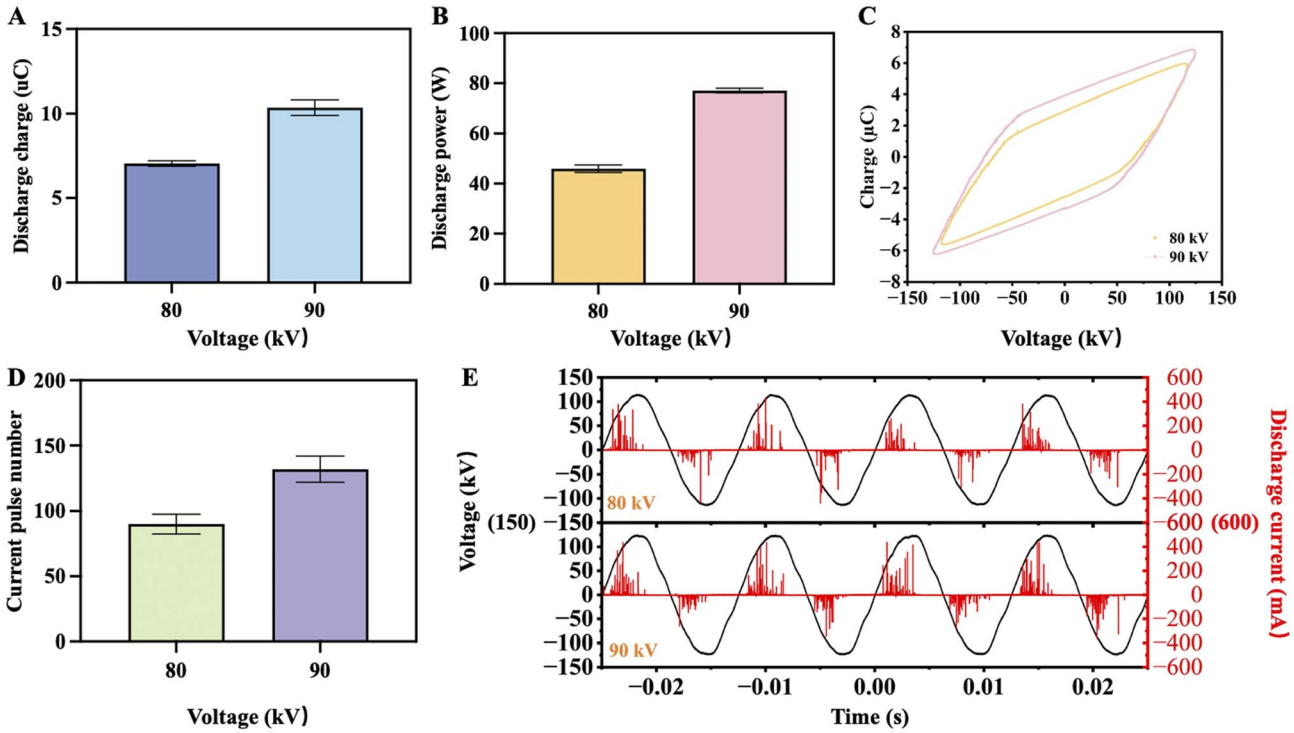

Fig. 13 Electrical characteristics and antimicrobial performance of the continuous in-package DBD cold plasma system: (A) discharge charge, (B) discharge power, (C) *Q*–*V* Lissajous loops, (D) current pulse number, and (E) *I*–*V* characteristics.

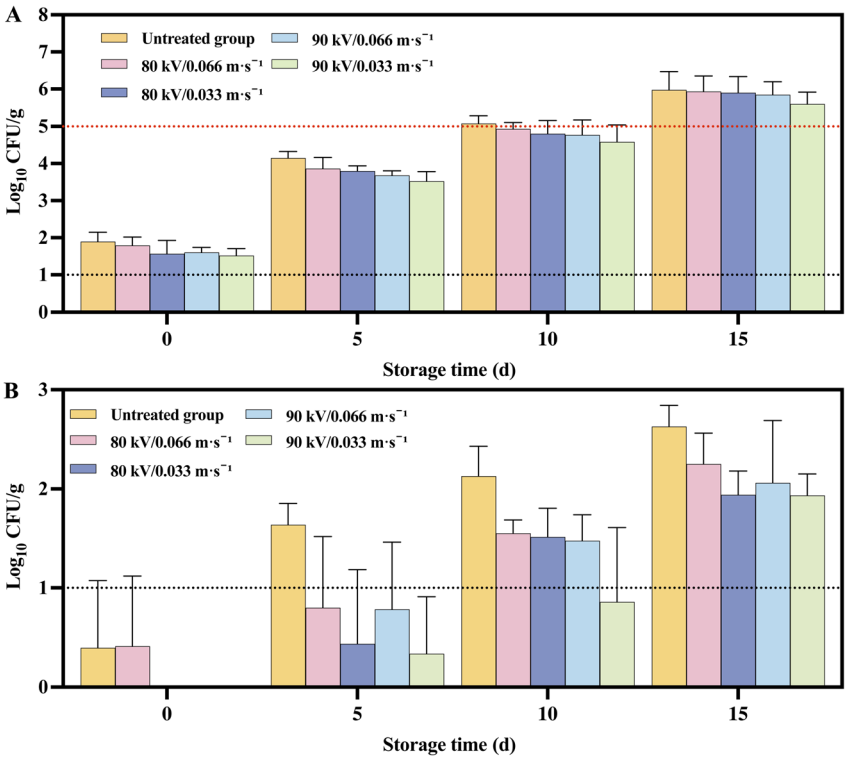

Fig. 14 Changes in (A) total plate count (TPC) and (B) molds and yeast counts of large-package fresh wet rice noodles (FWRNs) with or without pilot-scale continuous in-package DBD cold plasma treatment during 4 °C storage.

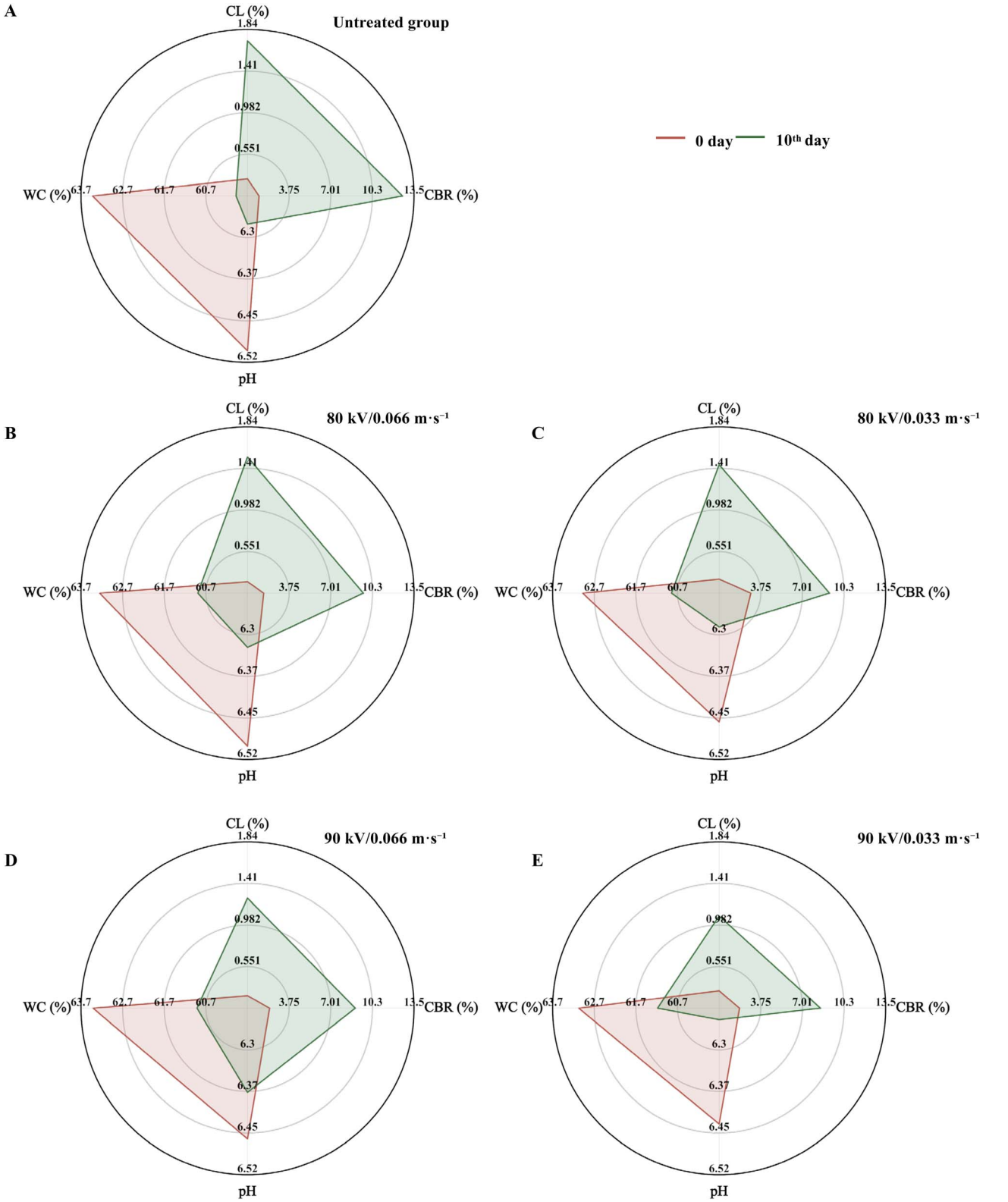

Fig. 15 Radar plot of quality attributes (CBR: cooked breakage rate; CL: cooking loss; WC: water content) of FWRNs during storage at 4 °C storage (day 0 and day 10): (A) untreated groups, (B) 80 kV/0.066 m s^{-1}, (C) 80 kV/0.033 m s^{-1}, (D) 90 kV/0.066 m s^{-1}, and (E) 90 kV/0.033 m s^{-1} treatments.

refrigerated storage. Regarding mold and yeast counts (Fig. 14B), after 15 days of storage, the untreated group increased to over 2.5 $\log_{10}$ CFU g^{-1}, while samples treated with in-package DBD cold plasma with 80 kV and 90 kV at a conveyor speed of 0.066 m s^{-1} reached 2.45 and 2.06 $\log_{10}$ CFU g^{-1}, respectively. When the conveyor speed was reduced to

0.033 m s^{-1}, mold and yeast counts were lower than 2 $\log_{10}$ CFU g^{-1}, which can be attributed to the longer treatment time.

In addition to microbial safety, key quality attributes of FWRNs that showed notable changes in previous experiment were further evaluated after 10 days of storage (Fig. 15). Compared with the untreated group, in-package DBD plasma treatments significantly reduced cooked breakage rate and cooking loss, indicating improved structural stability of large-package noodles. In addition, only minor variations were observed in water content and pH (6.25–6.38) among different plasma treatments, suggesting that the plasma process had limited impact on the basic physicochemical properties of the product under pilot-scale conditions. Regarding small-package FWRNs, pH values decreased to lower than 4.5 after plasma treatment (Fig. 9). However, such a pronounced reduction in pH was not observed in the large-package system. This difference may be attributed to the larger package volume and higher product mass, which could dilute or buffer the acidic reactive species generated by plasma, thereby reducing their overall impact on noodle pH.

4 Conclusions

In this study, an in-package DBD cold plasma system in vertical mode was used for the decontamination of FWRNs with emphasis on identifying scalable operating windows and key reactor parameters relevant to industrial implementation. The effects of applied voltage, dielectric barrier thickness, discharge gap, electrode area, and package atmosphere on electrical characteristics and microbial inactivation were comprehensively evaluated. The results indicate that, within a stable and controllable discharge regime, applied voltages above 70 kV, dielectric barrier thicknesses of 2–12 mm, discharge gaps of 30–45 mm, and electrode areas exceeding 50 cm^2 are found to be necessary to achieve sufficient discharge charge transfer and effective microbial inactivation. These parameter ranges indicate a practical engineering window for the design and scale-up of continuous, industrial in-package DBD cold plasma equipment. Additionally, O_2- and CO_2-containing atmospheres enhanced microbial decontamination efficacy compared with pure nitrogen, suggesting their potential for industrial package atmosphere selection (*e.g.*, air). During storage at 4 °C, in-package DBD cold plasma-treated FWRNs maintained TPC below 5 $\log_{10}$ CFU g^{-1} for >16 days, compared with approximately 6 days for conventional thermal pasteurization treatments. Furthermore, in-package DBD cold plasma-treated FWRNs retained better textural properties, cooking quality, and visual appearance during refrigerated storage. These findings establish links between reactor design parameters, discharge behavior, and decontamination performance, and provide a basis for developing scale-up equipment. With a conveyor system and extended electrodes, a pilot-scale in-package DBD cold plasma system was constructed for pilot-scale validation. It can effectively maintain the quality of large-package FWRN products while achieving microbial control at the pilot scale, supporting its feasibility for industrial application.

Author contributions

Hongyu Long: writing – original draft, formal analysis, investigation, data curation. Juhee Ahn: writing – review and editing, funding acquisition. Tian Ding: conceptualization, resources, review & editing of the final draft, supervision, funding acquisition. Xinyu Liao: conceptualization, resources, review & editing of the final draft, supervision, funding acquisition.

Conflicts of interest

The authors declare that they have no conflict of interest.

Data availability

All the data used in this study has been presented.

Acknowledgements

This work was financially supported by the National Key R&D Program of China (2023YFD2100802) and the Fundamental Research Funds for the Central Universities (226-2025-00220).

References

1 M. Li, M. Ma, K. X. Zhu, X. N. Guo and H. M. Zhou, *Food Chem.*, 2017, **216**, 374–381.
2 Z. Zeng, Q. Zhao, H. Wang, M. Lu, J. Fan, Y. Li, T. Zhou, X. Gong, C. Ren and X. Liu, *Int. J. Biol. Macromol.*, 2025, **328**, 147748.
3 M. Obadi, Y. Li and B. Xu, *J. Food Sci.*, 2023, **88**, 3626–3648.
4 X. Xiong, J. Wang, C. Liu, X. Zheng, K. Bian and E. Guan, *J. Food Process. Preserv.*, 2021, **45**, e15506.
5 Z. Wang, L. Han, A. Wu, P. Ma, J. Yang, C. Wang, Q. Shen and Q. Zhao, *J. Cereal Sci.*, 2025, **124**, 104219.
6 X. Liao, D. Liu, Q. Xiang, J. Ahn, S. Chen, X. Ye and T. Ding, *Food Control*, 2017, **75**, 83–91.
7 A. I. Muhammad, Q. Xiang, X. Liao, D. Liu and T. Ding, *Food Bioprocess Technol.*, 2018, **11**, 463–486.
8 T. Ding, P. J. Cullen and W. Yan, *Applications of Cold Plasma in Food Safety*, Springer, 2022.
9 R. Zhou, A. Rezaeimotlagh, R. Zhou, T. Zhang, P. Wang, J. Hong, B. Soltani, A. Mai-Prochnow, X. Liao, T. Ding, T. Shao, E. W. Thompson, K. Ostrikov and P. J. Cullen, *Trends Food Sci. Technol.*, 2022, **120**, 59–74.
10 D. Ziuzina, N. N. Misra, L. Han, P. J. Cullen, T. Moiseev, J. P. Mosnier, K. Keener, E. Gaston, I. Vilaró and P. Bourke, *Innovative Food Sci. Emerging Technol.*, 2020, **59**, 102229.
11 N. N. Misra, X. Yepez, L. Xu and K. Keener, *J. Food Eng.*, 2019, **244**, 21–31.
12 Y. Zhang, Y. Lei, S. Huang, X. Dong, J. Huang and M. Huang, *Food Sci. Hum. Wellness*, 2022, **11**, 845–853.
13 R. Moutiq, N. N. Misra, A. Mendonça and K. Keener, *Meat Sci.*, 2020, **159**, 107942.
14 P. A. Klockow and K. M. Keener, *LWT–Food Sci. Technol.*, 2009, **42**, 1047–1053.

15 N. N. Misra, K. M. Keener, P. Bourke, J. P. Mosnier and P. J. Cullen, *J. Biosci. Bioeng.*, 2014, **118**, 177–182.
16 A. S. Chiper, W. Chen, O. Mejlholm, P. Dalgaard and E. Stamate, *Plasma Sources Sci. Technol.*, 2011, **20**, 025008.
17 I. Albertos, A. B. Martin-Diana, P. J. Cullen, B. K. Tiwari, K. S. Ojha, P. Bourke and D. Rico, *Innovative Food Sci. Emerging Technol.*, 2019, **53**, 85–91.
18 H. J. Kim, H. I. Yong, S. Park, K. Kim, W. Choe and C. Jo, *Food Control*, 2015, **47**, 451–456.
19 H. I. Yong, H.-J. Kim, S. Park, A. U. Alahakoon, K. Kim, W. Choe and C. Jo, *Food Microbiol.*, 2015, **46**, 46–50.
20 J. H. Kang, Y. J. Jeon and S. C. Min, *Food Sci. Biotechnol.*, 2021, **30**, 1535–1542.
21 H. S. Lee, H. Lee, S. Ryu, S. Eom and S. C. Min, *Int. J. Food Microbiol.*, 2023, **389**, 110108.
22 D. Ziuzina, N. N. Misra, P. J. Cullen, K. M. Keener, J. P. Mosnier, I. Vilaró, E. Gaston and P. Bourke, *Plasma Med.*, 2016, **6**, 397–412.
23 X. Yang, J. Li and J. H. Cheng, *Food Res. Int.*, 2025, **221**, 117307.
24 National Health Commission of the People's Republic of China and State Administration for Market Regulation, *GB 4789.2-2022*, 2022.
25 National Health Commission of the People's Republic of China and China Food and Drug Administration, *GB 4789.15-2016*, 2016.
26 Y. Chen, G. Chen, R. Wei, Y. Zhang, S. Li and Y. Chen, *Food Chem.*, 2019, **297**, 124900.
27 Q. Wei, Y. Yuan, H. Gu, V. Raghavan, J. Zhang and J. Wang, *Food Control*, 2024, **160**, 110349.
28 J. Chen, X. Zhao, S. Li and Z. Chen, *Food Res. Int.*, 2024, **175**, 113727.
29 R. Dange, D. Sinausia, A. Bekkerman, D. Leybo and C. Vogt, *Green Chem.*, 2026, **28**, 1555–1565.
30 B. Wang, X. Wang and H. Su, *Plasma Chem. Plasma Process.*, 2020, **40**, 1189–1206.
31 S. B. Shim, S. Y. Cho, D. K. Lee, I. C. Song, C. H. Park, H. J. Lee and H. J. Lee, *Thin Solid Films*, 2010, **518**, 3037–3041.
32 U. Kogelschatz, *Plasma Chem. Plasma Process.*, 2003, **23**, 1–46.
33 J. Jung, C. Cho, M. Choi, S. You, J. Ha, H. Lee, C. Kim, I. Oh and Y. Lee, *Sensors*, 2023, **23**, 7121.
34 M. Abdollahzadeh, F. Rodrigues, J. Nunes-Pereira, J. C. Pascoa and L. Pires, *Sens. Actuators, A*, 2022, **335**, 113391.
35 H. Shang, H. Tang, X. Wen, W. Ning, X. Huang, S. Shen and S. Jia, *Plasma Processes Polym.*, 2025, **22**, e70073.
36 L. Han, D. Boehm, E. Amias, V. Milosavljević, P. J. Cullen and P. Bourke, *Innovative Food Sci. Emerging Technol.*, 2016, **38**, 384–392.
37 B. Yadav, A. C. Spinelli, N. N. Misra, Y. Y. Tsui, L. M. McMullen and M. S. Roopesh, *J. Food Sci.*, 2020, **85**, 1203–1212.
38 M. López, T. Calvo, M. Prieto, R. Múgica-Vidal, I. Muro-Fraguas, F. Alba-Elias and A. Alvarez-Ordóñez, *Front. Microbiol.*, 2019, **10**, 622.
39 E. Carini, E. Vittadini, E. Curti, F. Antoniazzi and P. Viazzani, *Food Chem.*, 2010, **122**, 462–469.
40 C. C. Qiao, X. H. Tian, L. X. Wang, P. Jiang, X. T. Zhai, N. N. Wu and B. Tan, *J. Cereal Sci.*, 2022, **104**, 103434.
41 M. Peleg, *Appl. Microbiol. Biotechnol.*, 2022, **106**, 1375–1382.
42 S. J. Wang, C. L. Li, L. Copeland, Q. Niu and S. Wang, *Compr. Rev. Food Sci. Food Saf.*, 2015, **14**, 568–585.
43 M. Bayati, M. N. Lund, B. K. Tiwari and M. M. Poojary, *Compr. Rev. Food Sci. Food Saf.*, 2024, **23**, e13376.
44 W. Yang, K. Zhu and X. Guo, *Foods*, 2022, **11**, 3093.
45 M. Ojukwu, J. S. Tan and A. M. Easa, *J. Food Sci.*, 2020, **85**, 2720–2727.
46 S. G. Kishore, M. Dwivedi, R. Rahul, J. Deepa, G. Jeevarathinam, K. Kamaleeswari, G. Jothiprakash and A. Veluswamy, *Sustainable Food Technol.*, 2026, **4**, 1057–1072.
47 R. Hoover, *Food Rev. Int.*, 1995, **11**, 331–346.
48 G. Guo, D. S. Jackson, R. A. Graybosch and A. M. Parkhurst, *Cereal Chem.*, 2003, **80**, 437–445.
49 M. Li, S. Dhital and Y. Wei, *Compr. Rev. Food Sci. Food Saf.*, 2017, **16**, 1042–1055.
50 Y. Kim, J. I. Kee, S. Lee and S. H. Yoo, *Food Chem.*, 2014, **145**, 409–416.
51 W. Xiao, Y. Q. Ding, Y. Cheng, S. L. Xu and L. Z. Lin, *Foods*, 2022, **11**, 2130.
52 W. Xue, C. Zhang, K. Wang, M. Guang, Z. Chen, H. Lu, X. Feng, Z. Xu and L. Wang, *Food Chem.*, 2021, **342**, 128321.
53 X. Yan, H. Xiao, J. Ye, S. Luo and C. Liu, *Foods*, 2025, **14**, 1079.
54 R. Rezler and S. Poliszko, *Food Hydrocolloids*, 2010, **24**, 570–577.
55 Ministry of Industry and Information Technology of the People's Republic of China, *QB/T 2652-2025*, 2025.
56 L. Gao, M. Guan, Y. Qin, N. Ji, Y. Wang, Y. Li, M. Li, L. Xiong and Q. Sun, *Int. J. Biol. Macromol.*, 2024, **262**, 129693.
57 M. Obadi, Y. T. Li and B. Xu, *J. Food Sci.*, 2023, **88**, 3626–3648.